1.2. THE PHYSICS OF CONDENSED MATTER

1.2.1. EXPERIMENTAL STUDIES

Experiments in the physics of condensed matter are mainly conducted with the spectrometers at the IBR-2 reactor. The EG-5 electrostatic generator and the DRON-4 X-ray diffractometer have also been utilized during the past two years for the certification of samples and for solving certain special problems.

At present, 10 spectrometers have been put into operation on eight beams of the IBR-2: HRFD, DN-2, HRNS, SNIM, DIFRAN, MURN, DIN, KDSOG-M, NERA-PR, SPN-1. During the period dealt with in the report new results have been obtained in all sections of PCM research under development at FLNP.

Diffraction. Studies of HTSC materials occupy a noticeable place among the investigations of structure.

A series of studies of the magnetic phase diagram of the HTSC $YBa_2(Cu_{1-x})Fe_x)_3O_{6+y}$ compound versus the concentration of iron, x, and the oxygen content, y, has been completed within a range of temperatures from 8 to 450 K. Experiments were carried out with the diffractometers of FLNP and LLB, Saclay, and, making use of the Moessbauer effect, at the IC RAS with samples enriched with the ^{57}Fe isotope. The high contrast achieved has permitted one the unambiguous determination of the probability of iron to substitute for copper atoms (Fig. 1), and to reveal the nature of the changes occurring at the interatomic distances (Fig. 2).

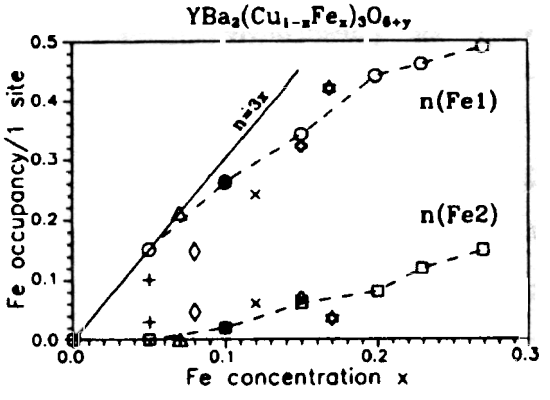

Fig. 1. Occupation factors of Cu1 and Cu2 positions in Y123-Cu/Fe by atoms of iron versus their concentration and in samples saturated with oxygen. Shown are the data of A.M.Balagurov et. al. (points O, □) and data in literature (the remaining points).

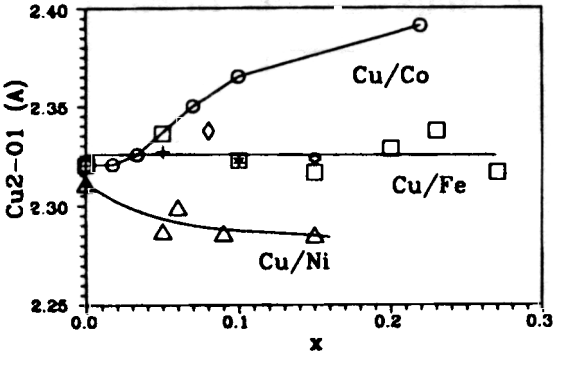

Fig. 2. Dependence of Cu2-O1 interatomic distance in Y123 on the concentration of impurity atoms: Fe, Ni, and Co. For Y123-Cu/Fe, data from literature are also presented. The size of the points corresponds to the errors.

Unlike the Y123 system, involving the substitution of cobalt for copper, the absence of a correlation between the temperature of the super-conducting transition and the Cu2-O1 interatomic distance was established. This lack of correlation was almost constant throughout the entire range of concentrations of the dopant atoms. This effect is in contradiction with the universal mechanism of

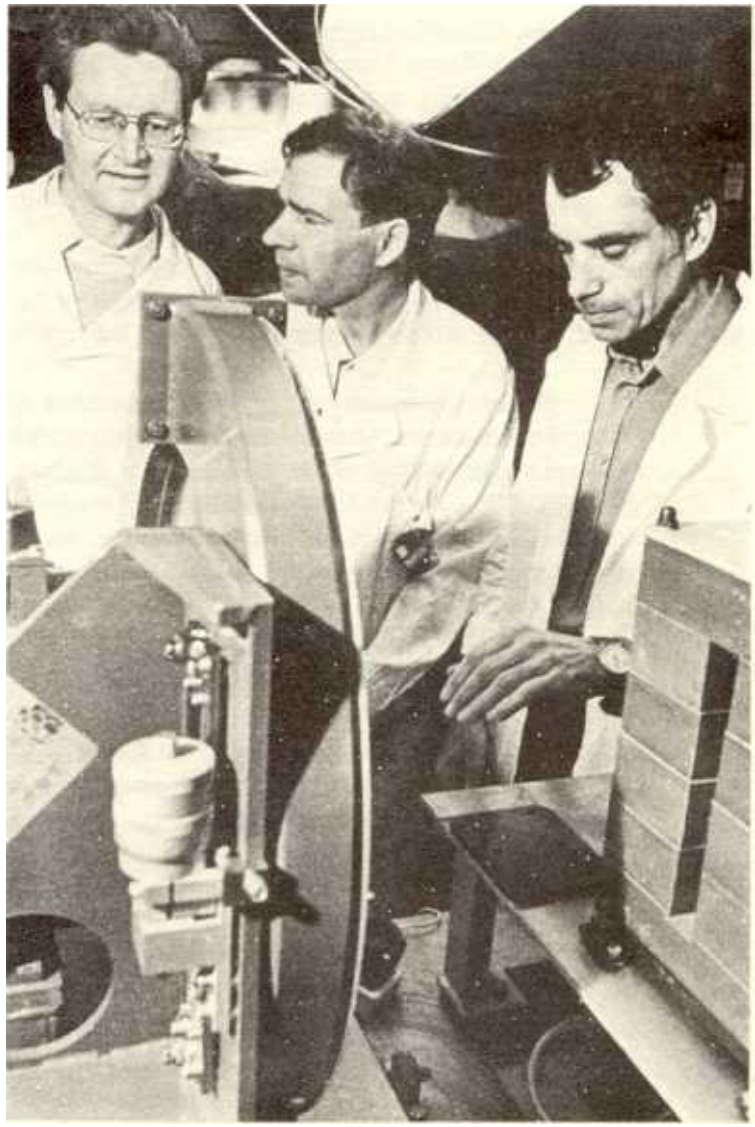

HRFD Fourier diffractometer on beam 5 at the IBR-2 reactor

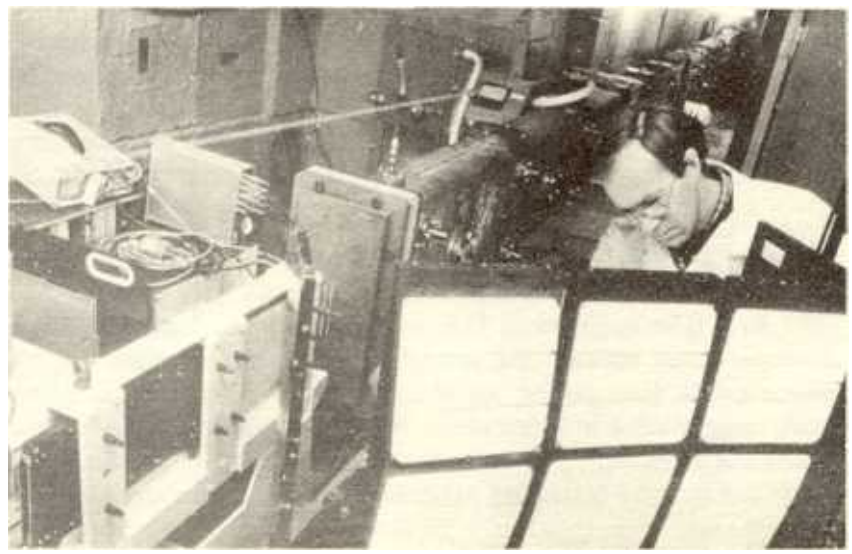

Neutron guide and Li-detector of HRFD

superconductivity loss in Y123 discussed in the literature. This effect is due to an enhancement of the interatomic distance and to the related transfer of negative charge from the chains in the plane, and points to processes taking place in the course of doping being more complicated than originally assumed. The magnetic phase diagram has been determined for the compound, meaning that domains have been established for the coexistence of superconductivity and magnetic ordering of the type of spin glass moments present in Cu-O chains, as well as the domains in which long-range antiferromagnetic order arises. The collinear antiferromagnetic structure existing for Fe concentrations exceeding 5% has been confirmed, together with a recovery behavior at temperatures below 100 K. In the region of iron concentrations of 7-23%, an unexpectedly strong coupling has been revealed between the spins of iron and copper, as well as a large magnetic moment induced at the Cu1 nodes.

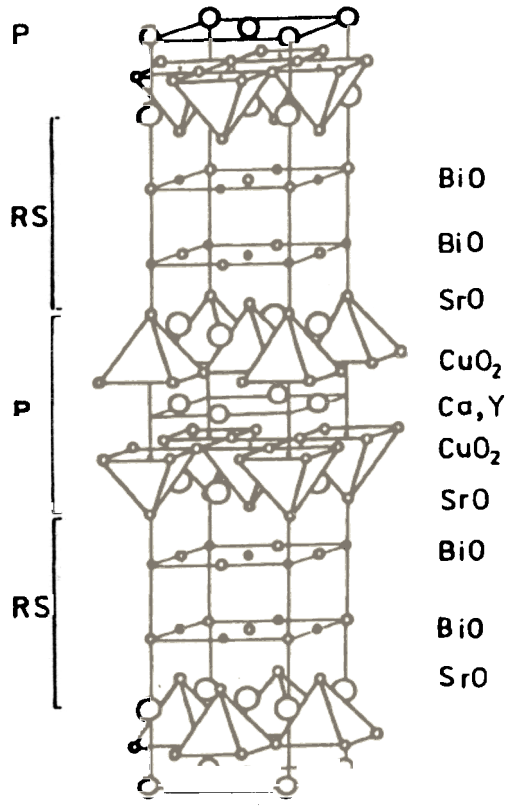

Fig.3. A simplified model of the $Bi_2Sr_2CaCu_2O_{8+\gamma}$ or $Bi_2Sr_2YCu_2O_{8+\gamma}$ structures.

Studies continued of modulated structures of Bi-superconductors. Owing to the complicated electronic configuration of the Bi^{3+} ion, it is precisely these HTSC compounds that exhibit a tendency towards the production of superstructures which might result in the formation of HTSC properties. The following systems were studied in experiments performed at the DN-2 diffractometer with mono- and polycrystals: $Bi_2(Sr, Ca)_3Cu_2O_{8+\gamma}$, $Bi_2Sr_{3-x}Y_xCu_2O_{8+\gamma}$ and $Bi_2Sr_2CuO_{6+\gamma}$. All these compounds were shown to exhibit structural modulation along the *a*-axis of an elementary cell. For concrete compositions of the systems indicated above, modulation was observed with periods of 4.25*a*, 4.75*a* and 5.0*a*, respectively. The structures of these compounds were determined (Fig. 3), and it was shown that the superperiod is due to the formation of $Bi_nO_{n+\gamma}$ chains along the *a*-axis (Fig. 4). Insertion of an additional oxygen atom (γ) into these chains leads to the appearance of wavelike displacements of the planes of atoms with amplitudes of 0.2-0.4 Å along the c-axis. Investigation of the temperature dependence of the modulation period and amplitude reveals no direct relationship with the superconducting properties of Bi compounds, but they determine, to a large extent, the balance of charge in an elementary cell. Thus, an extremely complicated structural problem found its solution in these experiments, which made possible an essential clarification of the situation with Bi compounds.

Of the numerous experiments performed by the method of diffraction in real-time mode, we note the work on phase states in titanium deuteride, TiD, carried out together with physicists of the SSPI, RAS (Chernogolovka). This work was the continuation of studies initiated in 1991 performed at temperatures between the temperature of liquid nitrogen and room temperature. This time, measurements were carried out at temperatures from room temperature up to 870 K. Thus, the entire range studied included about 700 K. Measurements showed that there were seven different phases and intermediate states with hcp, fcc, fco or bcc lattices of metal with deuterium atoms distributed over the octahedral or tetrahedral sites of the structure.

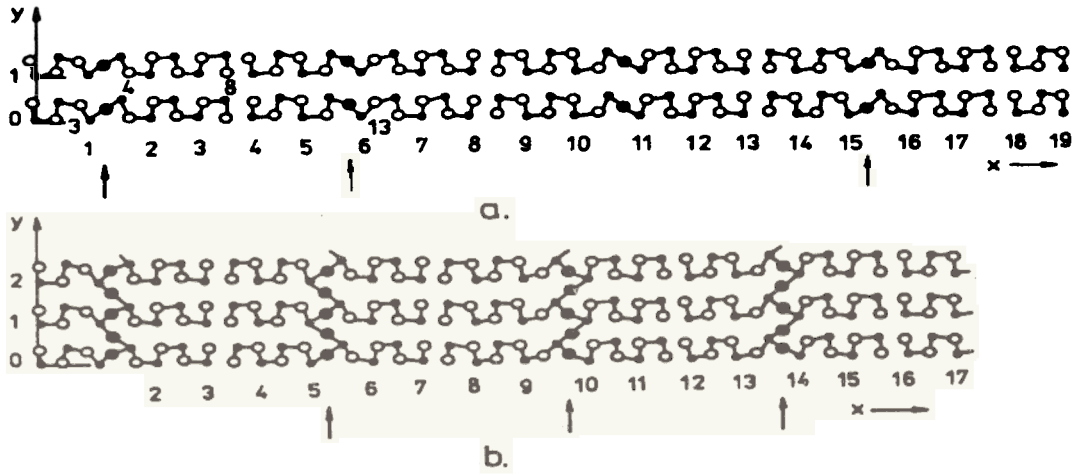

Fig. 4. Structure of $BiO_{1+0.5\gamma}$ planes in the 19a·b·c supercell of the $Bi_2Sr_{2.14}CaO_{0.72}Cu_2O_{8.21}$ compound (a) and 17a·b·c of the $Bi_2Sr_{2.4}Y_{0.6}Cu_2O_{8.5}$ compound (b) (Bi cations are indicated by black circles, the arrows point to the positions of the additionally inserted oxygen).

Formation of the Bi(Pb)-Sr-Ca-Cu-O HTSC compound was studied. For the first time it became possible to observe the formation and decomposition processes of the main phases of this system: 2201 and 2212 (Fig. 5). It has been shown that the intermediate $Sr_{1-x}Ca_xCuO_2$ phase plays an important part in these processes. At temperatures above 850°C the decomposition mechanism involves a process of partial melting. The stoichiometry that appears when the phase undergoes partial melting, determines the stoichiometry of the HTSC phase which forms when partial melting of the phase occurs. This, in turn, determines the stoichiometry of the HTSC phase which forms when the mixture cools slowly. The short annealing times of the produced phases permit formation of the 2212 phase. For formation of the 2223 phase, which exhibits a higher T_c, a more prolonged annealing is required. The work was carried out together with scientists from the Institute of Physics and Technology, Bucharest.

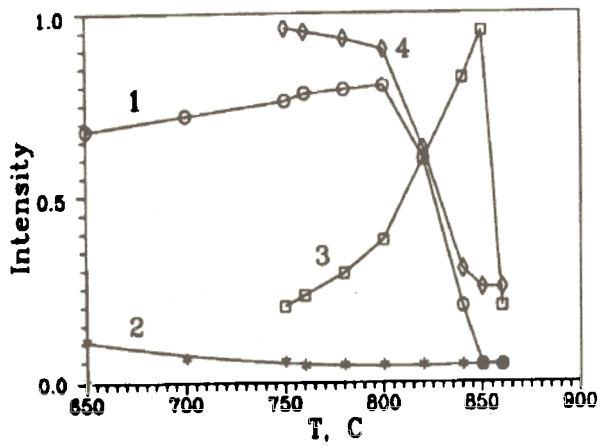

Fig. 5. Temperature dependence of the integral intensity of peak (002) for phases 2201 and 2212 in case of heating (curves 1 and 3) and cooling (curves 2 and 4), respectively.

Experiments are still under way for investigating structural phase transitions in ferroelectric and ferroelastic materials. A structural ferroelastic phase transition was observed in $RbLiH_3(SO_4)_4$ and the symmetry of the ferrophase was determined in a joint investigation carried out with the Institutes of Physics UAM (Poznan) and IPTM (Bucharest). Studies of the strontium-barium niobate ferroelectric were continued in collaboration with the MC, Rossendorf. In addition to the two high-temperature phase transitions studied previously, the existence of two low-temperature transitions was revealed, one of which is related to the rotation of the of which is related to the rotation of the ferroelectric axis through an angle of 90°.

Studies in the kinetics of the spin-flop transition in the antiferromagnetics Cr_2O_3 and α-Fe_2O_3 were continued with the SNIM-2 diffractometer equipped with a pulsed magnet. A hysteresis was observed in the dependence of the sublattice magnetization rotation angle upon the acting magnetic field (Fig. 6), in which the behavior of the antiferromagnetic when the the magnetic pulse field increases is found to differ from its behavior when the field decreases. The hysteresis phenomena are due to the following:

1) when the field variation is sufficiently rapid (~ $2x10^8$ Oe/s), the spin-flop transition proceeds adiabatically, i.e., the exchange of energy between the spin and phonon systems has no time to occur;

2) in the experiment, relaxation processes are observed that are related to the finite time (~10^{-5} s) required for establishment of an equilibrium state in the magnetic system, due to relativistic magnetic interactions.

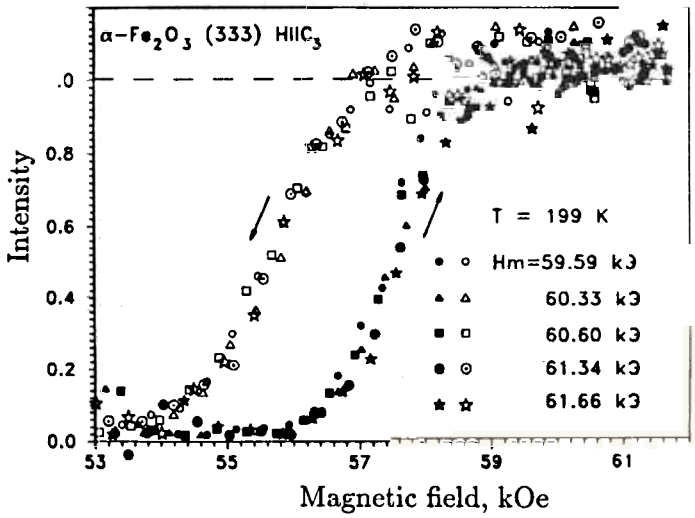

Fig. 6. Dependence of the diffraction peak (333) intensity of the α-Fe_2O_3 monocrystal on the pulsed magnetic field strength at a temperature of 199 K. The black dots correspond to the leading edge of the magnetic pulse, the light dots to the trailing edge.

Diffraction investigations have been made of a $HoFeO_3$ sample subjected to an external magnetic field. Antiferromagnetic ordering has been found in this rare-earth sublattice, which in the absence of the field is in a paramagnetic state. Studies were performed of this antiferromagnetic state. The sensitivity of the magnetic moment measurements amounted to 0.1 μ_B per cation. Temperature dependence of the "antiferromagnetic susceptibility" in the range from 79 to 220 K was measured. The noncolinearity of antiferromagnetic ordering in the iron sublattice was also determined and turned out to be 2%.

The HRNS textural diffractometer was used to obtain total pole figures from 42 samples of quartzites, gneisses, amphibolites and xenolites, including 12 samples from the Kola and German super-deep boreholes. Textures of artificially deformed quartzites and vanadium-titanium alloys were studied. This work was carried out in collaboration with scientists from Germany (from the Research Centre in Rossendorf, the Gottingen University, the Higher Technical School in Aachen and the Technical University of Klaustal) and Russian scientific centers (IEP RAS, GEOSYSTEM, MPII, UPI in Ekaterinburg, TTSU in Tula). Besides the above, measurements were performed of the form factors of liquid alkali metals (together with scientists of the Romanian IAP in Bucharest). Investigations were carried out of the distribution of atomic pairs in electric alloys (together with the Technical University in Kemnitz (Germany)) and the short-range ordering in oxide glasses (together with the University of Rostok (Germany)).

HRNS texture neutron diffractometer on beam 7a at the IBR-2 reactor

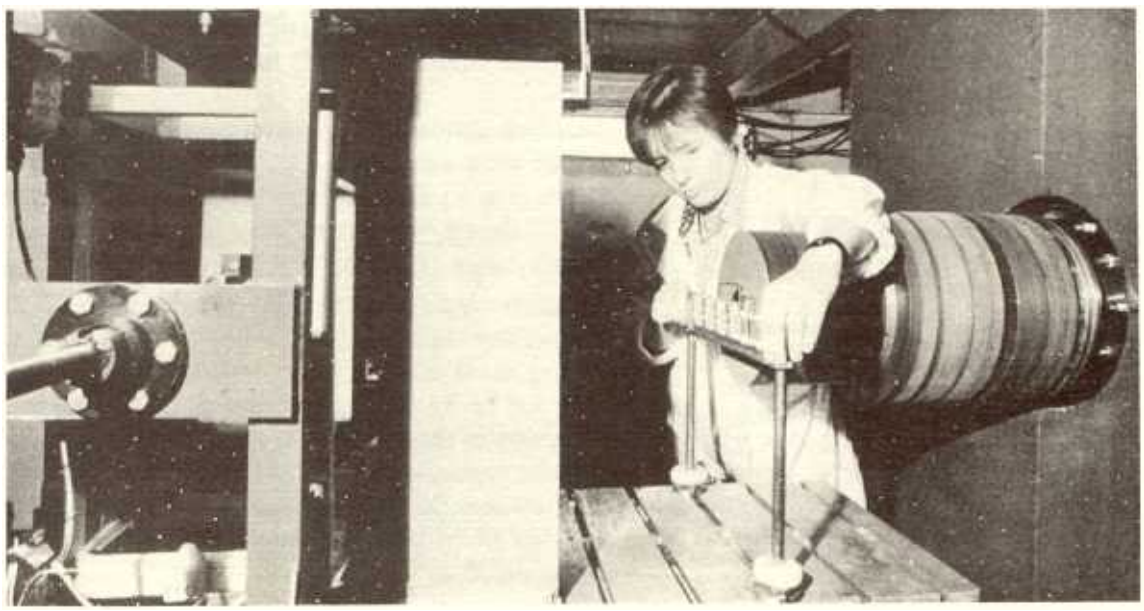

MURN small-scattering diffractometer on beam 4 at the IBR-2 reactor

Small-angle scattering. Intense studies were carried out with the MURN small-angle scattering spectrometer,.

A straightforward experimental comparison of MURN with one of the best spectrometers of this type, D-11 at ILL (Grenoble) was performed. Parallel measurements were carried out with samples composed of particles exhibiting an extremely wide spectrum of sizes. The following conclusions were made on the basis of a joint analysis of the measurement results: 1) the absolute intensities and inertia radii of both installations coincide within the errors; 2) the range of momentum transfers with MURN is 2 times wider than with D-11; 3) measurements of weakly scattering samples (with cross sections $\mu < 0.05$ cm^{-1}) take the same time with both instruments; 4) measurements of strongly scattering samples ($\mu > 0.1$ cm^{-1}) require significantly more time with MURN, than with D-11. The D-11 diffractometer, however, is about at its level of technical perfectness, while the commissioning of a cryogenic moderator at the IBR-2 reactor, as well as the nearly completed installation of a new position-sensitive detector at beam N 4 will essentially broaden the facilities of MURN by increasing in the spectral range and allowing better spatial resolution in the detection of scattered neutrons.

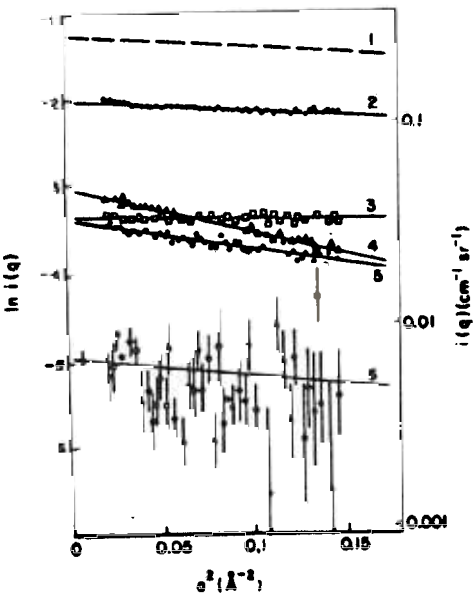

Fig. 7. Guignet curves obtained from measurements of neutron small-angular scattering on the MURN spectrometer: 1 - H_2O:D_2O solution = 1:1 (the experimental points are not presented); 2 - H_2O:D_2O = 1:4; 3 - vanadium sample 3 mm thick; 4 - solution (1M) H-TMU in D_2O; 5 - solution (1b) of mixture H- and D-TMU in H_2O-D_2O at 30 mol.% H_2O; 6 - solution (1M) H-TMU in H_2O-D_2O at 60 mol.% H_2O.

Various types of Portland cement were investigated, as well as their hydration in compounds. Dry cement was found to follow the Porod potential law, while compounds did not yield, in the measured Q-range, a similar behavior of small-angle scattering curves. Investigation of nuclear tracks in solid-state detectors by the method of small-angle neutron scattering was carried out in collaboration with FLNR JINR. RERT type foils of the were also studied. The irradiated foils displayed a Guignet-like behavior of the scattering curves. The measured radius of inertia turned out to be about 8 nm. Annealing (160°) lead to a decrease of the radius.

Searches continued for perturbation effects of the structure of a solvent in the vicinity of a dissolved molecule (Fig. 7). In collaboration with staff members of CIPR, Budapest, experiments were carried out with tetramethylurine (TMU), and the temperature and temperature and concentration dependences of the scattering law were obtained. Despite the fact that the scattering cross sections to be measured were small, it turned out to be possible to reveal the orientational perturbation of the structure of a solution in the vicinity of a TMU molecule and, also, to establish the existence of an attractive potential between the molecules, which arises due to hydrophobic interactions in accordance with assumptions.

For the first time studies were performed of micelle systems at high hydrostatic pressures. In solutions of tetradecildimethylaminoxide (C_{14}-DMAO) at pressures in ranges up to 8 kbar, a phase transition was found in which cylindrical micelles with radii of 18.5 Å and lengths of 160 Å undergo

transition to states with a 52 Å radius. The experiments were carried out together with physicists from Baireuth (Germany).

Inelastic scattering. New results in the molecular dynamics of condensed matter were obtained by the method of inelastic neutron scattering.

The DIN-2PR and DIN-2PI direct geometry spectrometers (monochromatization of the neutrons incident upon the sample) were, used for continued investigations of the dynamics of liquid helium, liquid metals and molecular liquids, as well as the dynamics of alloys and local oscillations of dopant hydrogen, nitrogen and oxygen atoms in metals and alloys.

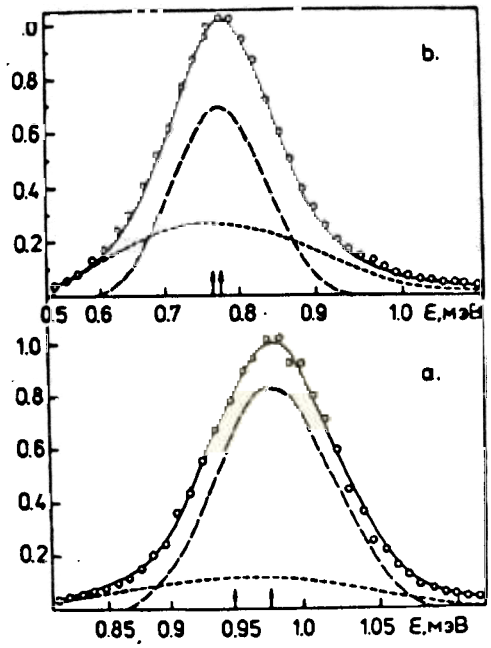

Fig. 8. Spectrum of neutrons back-scattered on He II: a - T = 1.4 K; E_0 = 2.05 meV; q = 1.6 Å^{-1}; b - T = 1.72 K; E_0 = 2.45 meV; q = 1.83 Å^{-1}. The solid line is a fit to the experimental data; the dashed lines indicate a decomposition into two Gaussians. The arrows point to the positions of the Gausssians.

The main accent in the investigation of the quantum properties of liquid helium-4 has shifted from studies of the momentum distribution of atoms by analysis of the spectra of neutrons scattered with large momentum transfers (the impulse approximation) to a detailed investigation of the dispersion curve of excitations in liquid helium at various temperatures. To perform the indicated research, the DIN-2 spectrometer operated at initial neutron energies below 2 meV. The low initial energies made possible an essential reduction of the influence of multiphonon and multiple scattering of neutrons and improvement of the resolution from 50 up to 100 meV depending on the energy transfer. A manifestation of the high sensitivity achieved was the observation of peaks related to neutron scattering in liquid helium involving acquirement of energy, i.e. of excitations present in the liquid. An analysis of the experimental spectra of inelastically scattered neutrons revealed that the phonon-maxon-roton peak has a complex multicomponent structure (Fig. 8).

At temperatures above the λ-point in the phonon region, excitations were observed that can be associated with long wave excitations such as the first or zeroth sound (Fig. 9, indicated by triangles).

At all wave vectors a broad peak is seen, the physical nature of which is not quite clear at present. It may be due to the quasicrystalline structure of the liquid or to neutron scattering on thermal excitations or to other mechanisms (full circles in Fig. 9). At temperatures below the λ-point, an additional branch is observed, besides the indicated branches,, which is the dispersion curve for quasiparticles and is related to the canonized Landau curve (open circles in Fig. 9). The temperature dependence of the relative intensity of scattering on quasiparticles repeats the behavior of the order parameter curve in liquid helium II.

The results show that, most likely, three different excitations exist in liquid helium-4, which manifest themselves in different ways, depending on the temperature and the wave vector. Here two characteristic regions of significant restructuring of the excitation energy spectra may be distinguished. First, strong qualitative and quantitative changes in the nature of neutron scattering occur within a very narrow temperature interval or actually at the point of transition to super-fluidity, T_λ. Second, explicit changes in the nature of excitations both in superfluid and in normal helium take place in a narrow range of wave vectors (0.5-0.65) Å^{-1} in the transition from phonons to maxons.

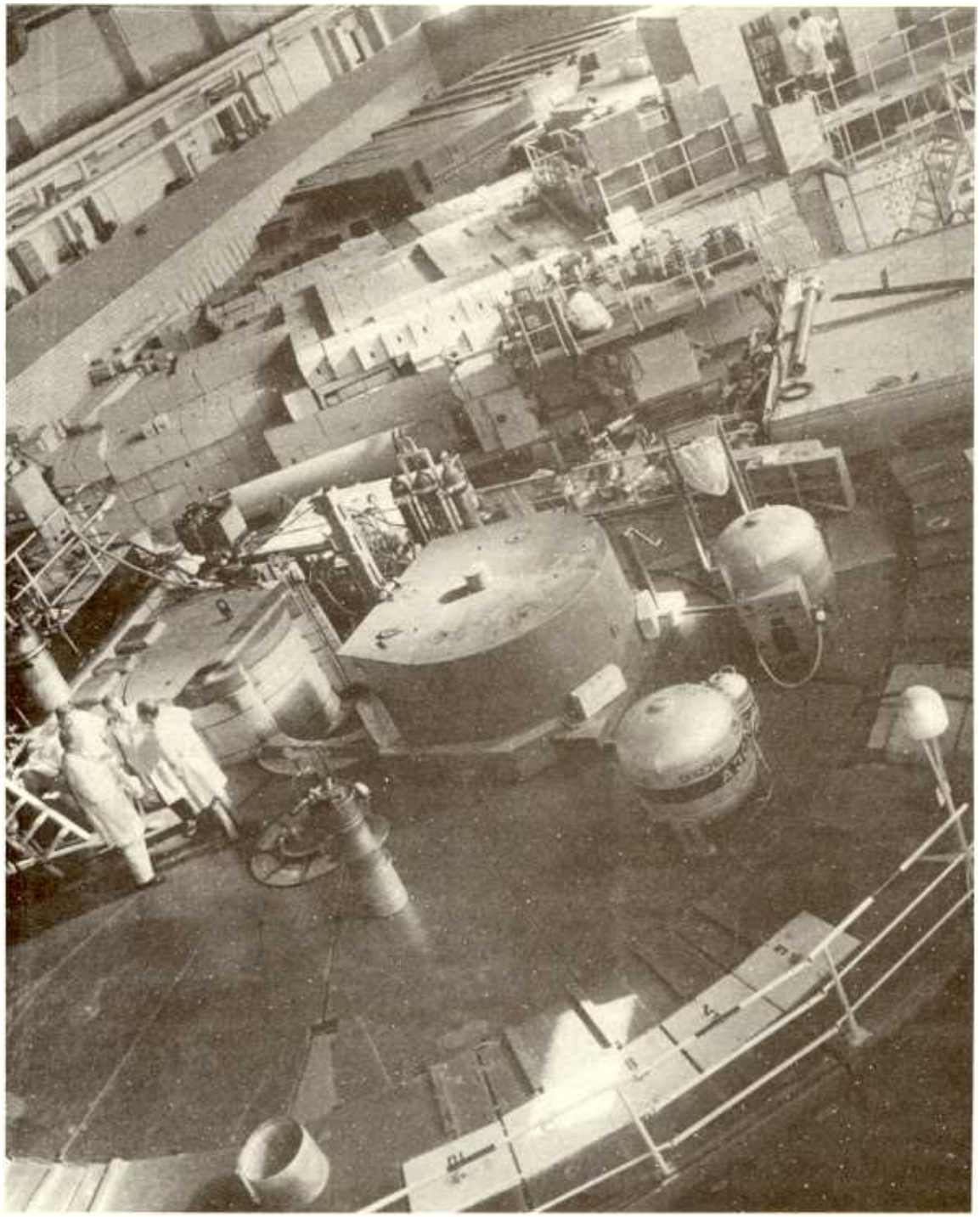

DIN-2PI inelastic scattering spectrometer of the direct geometry on beam 2 at the IBR-2 reactor

The issue of the amount of Bose-condensate in super-fluid helium-II is still under discussion, initiated by the works of F.London, N.N.Bogolubov and S.T.Belyaev. According to the Glide-Griffins concept, the intensity of the peak of quasiparticles is determined by the density of Bose condensate. Therefore, the experiments made it possible to apply an independent method for determining the density of Bose condensate.

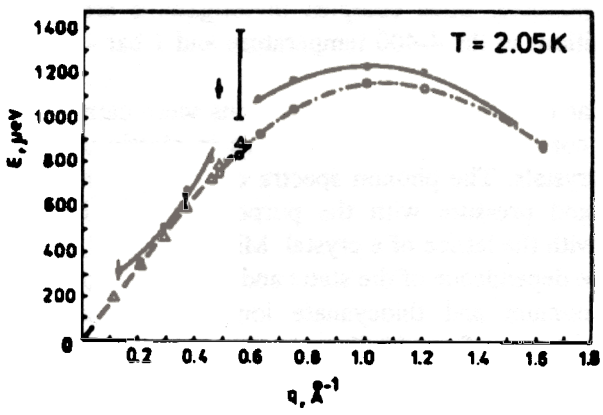

Fig.9. Dispersion curves for liquid helium-4 at a temperature of 2.05 K.

Studies of nitrous austenitic steels are under way to determine the force constants of interatomic interactions. Admixtures of nitrogen strongly influence the hardness of austentitic steels. The frequency spectra have been investigated for austenitic alloys Fe-Cr-Mn-Ni (f.c.c) with nitrogen contents in the range of 0.06-0.5 weight %. It was found that, unlike the nitrous chrome-manganic steels investigated previously, theaddition of nitrogen does not lead to a change in the Me-Me and Me-N force interaction, in the case of a Fe-18Cr-10Mn-16Ni compound. Studies were also performed of alloys of the $TaN_{0.45}$ and $NaN_{0.45}H_{0.1}$ β-phase intrusions. Data were obtained on the oscillation energies of nitrogen and hydrogen atoms and on constants of the force interaction of interstitial metal-atom interaction. Investigation has continued of double and triple hard interstitial solutions. The phenomenon of interstitial nitrogen atoms being "captured" by Ta-V substitution admixtures has been studied using the example of a $TaV_{0.03}N_{0.03}$ solution. Besides local nitrogen peaks in the frequency spectrum of the solution investigated, peculiarities were observed that were due to oscillations of vanadium atoms associated with the "captured" nitrogen atoms. Investigation of the structure of the admixture zone in the $YO_{0.03}H_{0.03}$ alloy revealed that the oscillations of interstitial hydrogen and oxygen atoms do not correspond to the location of these atoms at the centre of the octahedral inter-nodal position of the yttrium cubic lattice.

Spectra have been measured for inelastic neutron scattering on PbF_2 in the 293-773 K temperature interval with the aim of determining the density of phonon states at temperatures higher and lower than the super-ionic transition, $T_c \sim 700$ K.

Two-dimensional liquids have been studied, taking advantage of the example of water adsorbed on the surface of pyrogenous silica and porous silicon dioxide. Simulation of the quasielastic scattering law and analysis of the angular dependence yielded the self-diffusion coefficients of water molecules, the hydration shell of silica and of aerosil hydrogel, and the average square deviations of hydrogen atoms from equilibrium positions.

Studies were performed of the scattering of slow neutrons by liquid potassium in the 340-550 K temperature interval. A technique for taking coherent effects into account was elaborated on the basis of the Lovsee viscous-elastic model. Analysis of experimental spectra with the aid of the developed technique resulted in our obtaining the hitherto unavailable temperature dependence for the frequency spectrum of oscillations of atoms of the melt and for other microdynamic characteristics related to this spectrum: autocorrelation speed function, root-mean-square oscillation amplitude of atoms averaged over the direction of the force constant of interatomic interactions, and, also, the calculated isochronic heat capacity taking into account anharmonic effects. The characteristics were obtained for diffusion processes in liquid potassium in the indicated temperature

range together with an idea of the mechanism governing these processes. The correspondence of the experimental results with the theory of interaction between modes was investigated. Collective modes in liquid helium were investigated, and these data were used to calculate the lifetime and non-Markovian behavior criteria characteristics of relaxation processes in a melt:.

The KDSOG and NERA-PR inverted geometry spectrometers make simultaneous studies of inelastic scattering and diffraction of neutrons possible. Such complex investigations are being successfully implemented for studying phase transitions in the 4-400 temperature and 1 bar - 1 kbar pressure ranges.

Investigations of the dynamics of molecular crystals and phase transitions were carried out with the NERA-PR spectrometer. Studies were continued of phase transitions in plastic crystals, such as camphor, and other types of molecular crystals. The phonon spectra of meta-, ortho- and paraxylene were measured versus temperature and pressure with the purpose of studying the dynamics of methyl groups and their interactions with the lattice of a crystal. Mixed $K_{1-x}(NH_4)_xSCN$ crystals were used for investigating the temperature dependence of the static and dynamic disorder of ammonium and thiocyanate ions in the range of temperatures from 10 K up to room temperature and in a broad range of ammonium concentrations. Several phase transitions were revealed that are related to the dynamics of ammonium ions: a structural phase transition of the order-disorder type at low temperatures for x = 0.75, a transition from dynamic reorientation to the phase of proton glass for $0.3 < x < 0.75$ and to the phase of nearly free quantum rotation at helium temperatures for $x < 0.1$.

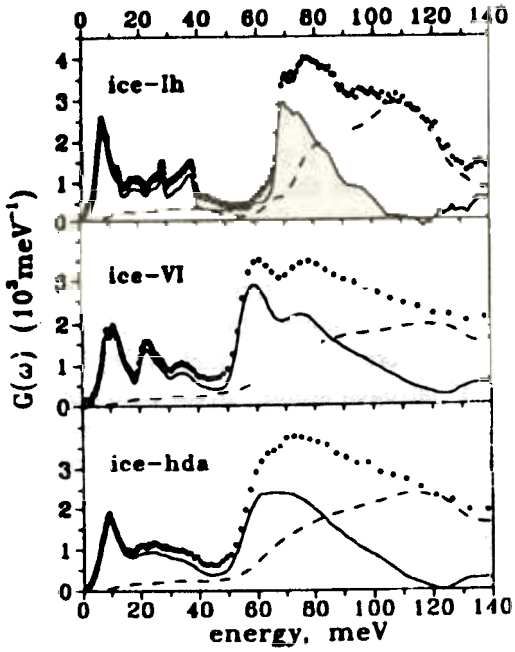

Fig. 10. Plots of generalized vibrational density of states G(ω) for hexagonal H_2O-ice Ih, the quenched high pressure phase VI, and amorphous ice of high density (hda). The points indicate the overall experimental spectrum, the dashed lines show theoretically calculated contributions of multiphonon neutron scattering; the solid lines are one phonon spectra.

The good resolution that can be achieved with the NERA-PR spectrometer was used for investigations of both lattice dynamics and internal molecular oscillations of a series of amino acids with the purpose of determining the characteristic oscillation frequencies of the CH_3 and NH_3 molecular groups. Owing to the large scattering cross sections of neutrons on protons, the dynamics of these groups is manifested clearly in neutron spectroscopy.

The vibrational spectrum of quenched amorphous ice of high density (hda), obtained by compressing hexagonal Ih ice up to 13 Kbar at 77 K, was studied with the aid of inelastic incoherent neutron scattering in the energy region from 1 to 120 meV at 80 K (Fig. 10). The spectra of Ih ice and of the quenched high-pressure phase IV ice were also measured for comparison. In the translational zone of the hda ice phase spectrum, the first peak in the region of acoustic modes is shifted by 2 meV towards higher energies, as compared to Ih ice, while in the tortional zone the spectrum reveals that the low-energy cutoff of this zone is shifted by 13 meV toward low energy transfers. The principal characteristics peculiar to the spectra of hda ice and of ice IV were observed to be similar, thus indicating that the dynamics of these phases must depend on the same atomic correlations and force constants.

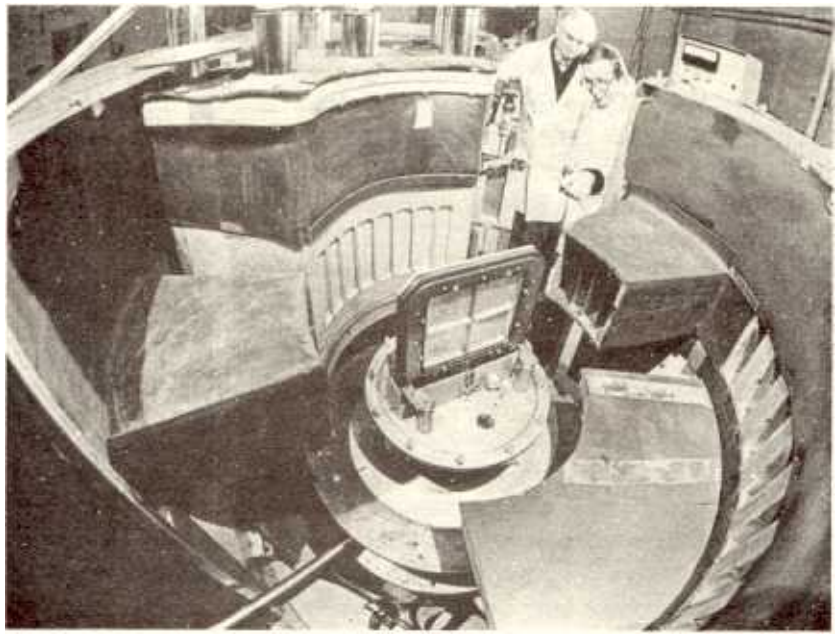

NERA-PR inelastic scattering spectrometer of inverted geometry on beam 7b at the IBR-2 reactor

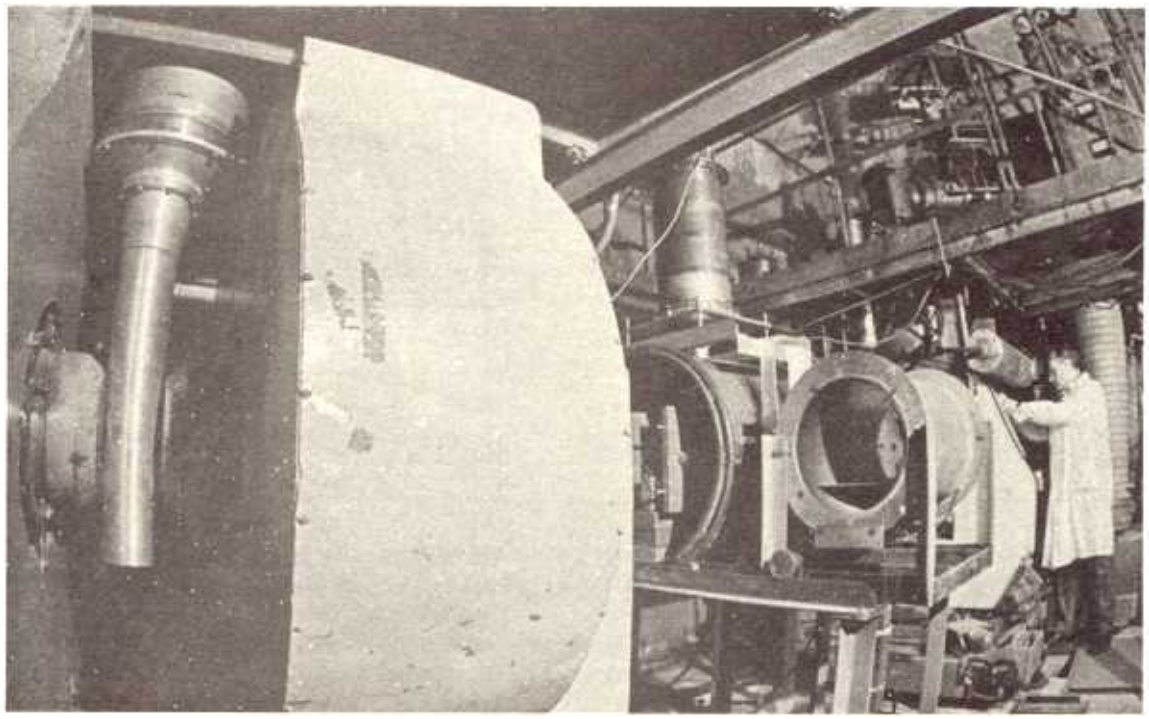

POLYANA spectrometer for experiments with polarized neutrons and nuclei on beam 4 of the IBR-30 booster

Vibrational spectra of finely granulated silicates and of water adsorbed on them were studied with the KDSOG spectrometer. The results are used for clarifying the microscopic mechanisms of water adsorption on the surface of silicates. Generally, this spectrometer is used for studies of crystalline fields in alloys and compounds of rare-earth elements. A series of experiments has been carried out to studyi the crystal electric field (CEF) in $ReCu_2Si_2$ compounds (Re = Ce, Nd, Pr, Er, Tb, Ho, Yb). The dependence of the parameters on Re was determined. The spectra of magnetic excitations in systems with intermediate valence (IV), CeNi, Ce(La, Y)Ni and PrCe(La, Y)Ni, were studied with the purpose of investigating the CEF transformation in transition from IV to the Condo mode of the 4f-electron shell.

Polarized neutrons. The SPN-1 polarized neutron spectrometer was used for continuing studies of the magnetic properties of thin and multilayer films by the method of specular reflection.

The profile of the constant magnetic field penetrating into superconducting niobium films (Fig. 11) was measured. At a temperature of 4.9 K, a 500 Gauss field within the limits of ξ = 28 nm penetrated the superconductor at the boundary with vacuum practically without damping, which is related to the near-surface suppression of the order parameter of the superconductor. Deeper in the film the damping follows the London law with a constant Λ = 45 nm. By the improved method of inverse resonance scattering of accelerated helium ions on oxygen it turned out to be possible to establish the existence of a natural 5 nm thick NbO oxide at the surface of the niobium superconductor film being studied with the aid of neutrons. Observation of the oxide confirms the existence of a hitherto unknown mechanism for the origination of the normal phase at a real microcoarse boundary with a vacuum.

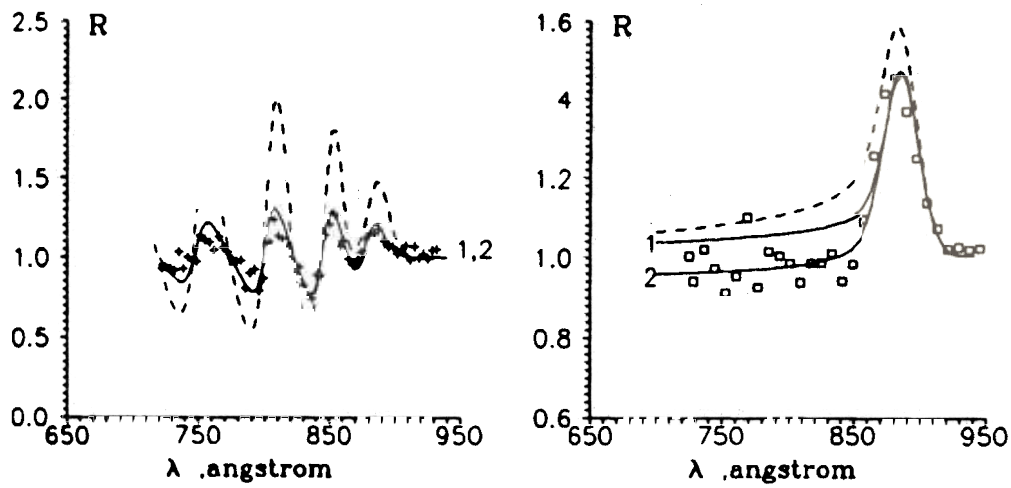

Fig. 11. Experimental ratio R of the reflection coefficients of neutrons with opposite polarizations versus the normal to the film plane component of the neutron wavelength λ: the crosses indicate a thin film, the squares a thick film. The dashed line is calculated within the London model for Λ = 43 nm. The solid line indicates: 1 - calculation within the London model for the best fit and Λ = 95 and 90 nm for the thin and thick films, respectively; 2 - calculation by the model with inclusion of a dead layer at the boundary of the film (a solution consistent for both films has been obtained with ξ = 28 nm and Λ = 45 nm).

It has been demonstrated and experimentally proven that single-axis anisotropic magnetic films exhibit a sufficiently large coercive force to create neutron beams of differing polarizations, depending on the orientation of a weak external magnetic field relative to the magnetization vector of the film (Fig. 12). This makes it possible to use them as wide-spectrum neutron polarizers in neutron polarization spectrometers without applying spin-flippers.

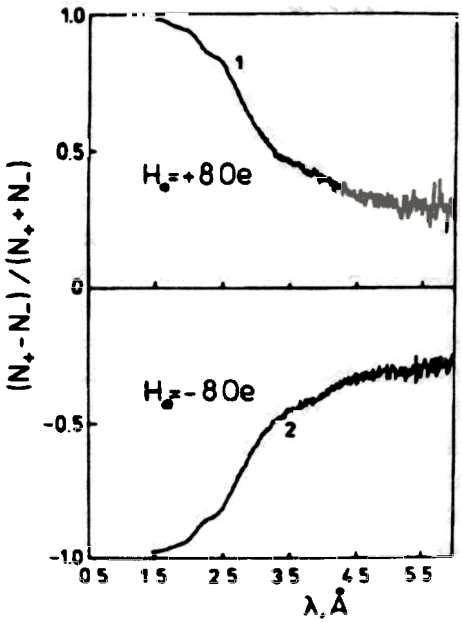

Fig. 12. Experimental dependence of the quantity $P_0P = (N_+-N)/(N_++N)$, where P_0 is the incident beam polarization, P is the polarizing power of the film, upon the neutron wavelength λ for a FeCo film with a rectangular hysteresis loop: 1 - orientation of external magnetic field parallel to the film magnetization; 2 - antiparallel.

The first experiments have been performed in search of an induced magnetic moment in a non-magnetic medium adjacent to the magnetized medium. Measurements were performed with a series of Pd/Co (20 Å)/Pd samples (Fig. 13). The magnetic moment in the Co layer turned out to be 1.7 μ_B. No moment was found to appear in the Pd layer, the upper limit imposed on its value was $\mu < 0.4\ \mu_B$. The aim of another investigation was to study ferro- and antiferromagnetic exchange interactions in coupled films. These investigations are of great interest for clarifying the nature of the giant magnetoresistance in such films. Unlike optical and magnetometric methods, the method of neutron reflection permits a determination of the value and orientation of the magnetization vector in each individual layer. The first experiments were carried out with Co/Cu/Co samples with Cu thicknesses of 9 and 13 Å. An unusual behavior of these epitaxial structures was observed, which demonstrate a very weak or practically zero antiferromagnetic pairing between the magnetic and non-magnetic layers. Ferromagnetic interaction had already been observed in the case of weak external magnetic fields: at 30 Gauss the magnetic moment per 1 Co atom amounted to 1.1 μ_B. When the external field was increased up to 1.4 kGauss, only a weak enhancement of the magnetization in these films was observed (up to 1.3 μ_B per 1 Co atom). The issue of the relationship between this increase in magnetization and the giant magnetoresistance observed in this range of magnetic fields remains unclear.

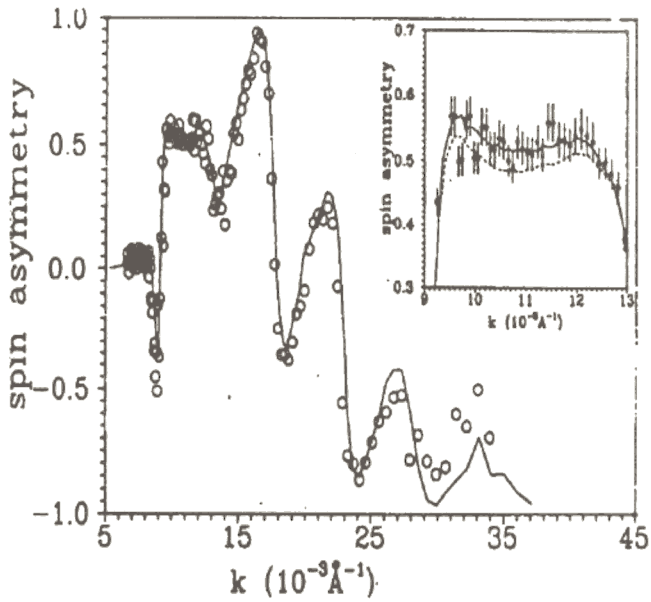

Fig. 13. Dependence of spin asymmetry $SA = (R_+-R)/(R_++R)$ in reflection of polarized neutrons on the normal component of the neutron wavevector K for a Pd/Co/Pd film, deposited on the surface of silicon with a sublayer of gold: the dots represent the experiment, the line - calculations of $\mu_{Co} = 1.73\ \mu_B$ and $\mu_{Pd} = 0.4\ \mu_B$ in a layer 5 Å thick at each Co/Pd boundary. Both lines in the insertion are computed; solid line - $\mu_{Co} = 1.8\ \mu_B$; dashed line - $\mu_{Co} = 1.73\ \mu_B$ (corresponds to a massive sample).

The SPN-1 spectrometer provides good possibilities for applying the method of neutron depolarization to the study of magneto-inhomogeneous media. The spectral function of depolarization contains information both on the parameters of magnetic inhomogeneities (size, spread of magnetization orientations) and on the nature of pair correlations between local magnetization vectors in adjacent microregions. Manifestations of the information on correlations should depend on the depolarization function $D(\lambda)$, and on the neutron path length d in the sample, which can be altered by rotating the sample through an angle θ about the axis coinciding with the direction of the magnetic field. In the Halpern-Holstein theory there exists a constant, $f = D_1(\lambda)^{d2(\theta 2)/d1(\theta 1)}/D_2(\lambda)$, independent of the neutron wavelength. However, in the case of samples exhibiting a correlation between mutual orientations of the micromagnetization, or in the case of samples with micromagnetic elongated inhomogeneities packed anisotropically, the value of f depends on the neutron wavelength. Fig. 14 presents experimental data for a thin laminated steel ribbon. The form of function $f(\lambda)$ points to the packing of the magnetic particles elongated in a direction perpendicular to the rolling. The function $f(\lambda)$ obtained for annealed Permalloy (Fig. 15) confirms the absence of pair correlations between the orientations of local magnetizations and, also, of any priority orientation in the packing of magnetic particles. Inclination of the plane of a thin sample relative to the external field allows the defining of an initial polarization, P_0, at the entrance to the sample, that differs in orientation from the induction vector within the sample. In this case the depolarization process is complemented by rotation of the vector, P, about the induction vector, as in the technique of three-dimensional polarization analysis. An example of a depolarization curve obtained by transmission through an inclined sample of transformer iron is presented in Fig. 16. In this case the function $P(\lambda)$ is most informative since it allows spectral analysis to be performed simultaneously with the three polarization vector components at the exit from the sample.

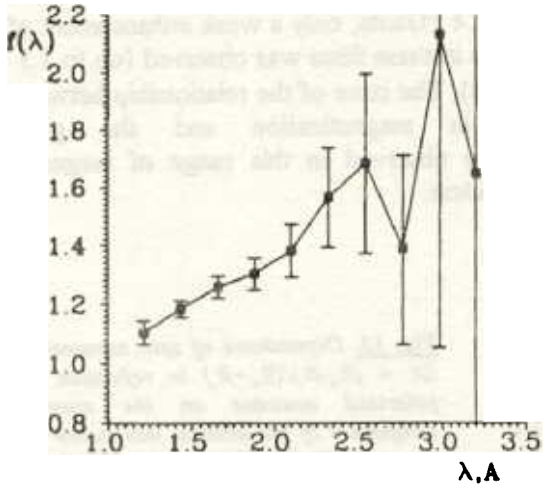

Fig. 14. Shape of function f(λ), measured for a thin rolled steel ribbon 300 μm thick in an external field of 160 Oe.

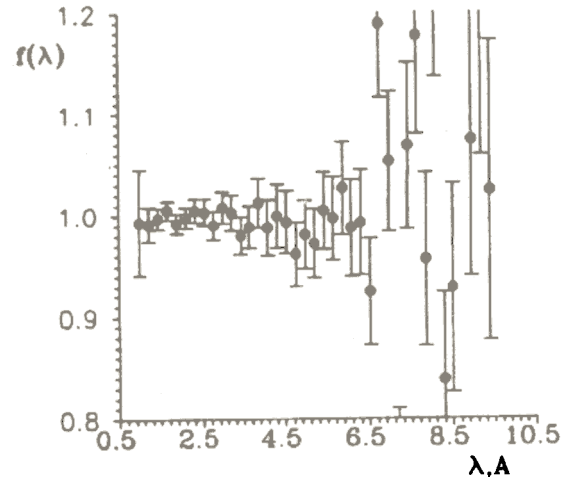

Fig. 15. Shape of function f(λ) for an annealed Permalloy ribbon 160 μm thick.

Systematic investigation was performed of the dependence of neutron depolarization in samples of HTSC ceramics Y123 (T_c = 91 K) upon temperature (77-250 K) and the external magnetic field. The most interesting temperature region is found around T_c, where theory predicted new magnetic phenomena such as: transition of the vortex lattice into the spin-glass state, melting of the vortex lattice and others, which may be manifested in specific behavior of the neutron

depolarization when the temperature and external field undergo variations. New information has been obtained on the magnetic field distribution in a sample. Thus, for example, a possible manifestation was found of the so-called depinning line, which separates captured and freely moving vortexes.

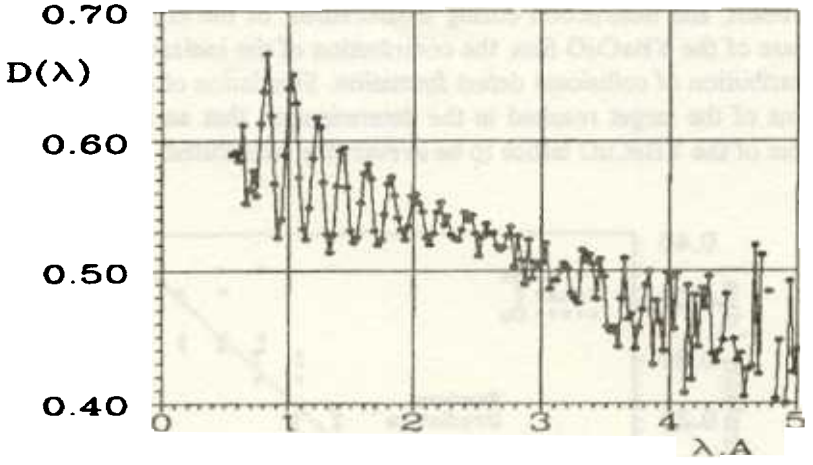

Fig. 16. *Depolarization function D(λ) measured with the aid of neutron transmission through an inclined sample of transformer iron 300 μm thick. The angle between the axis of the sample and the external field (460 Oe) equals 10 °.*

Scattering of accelerated helium ions. New possibilities for investigating the structure of HTSC materials opened up with the application of a combination of channeling and inverse-scattering methods at the EG-5 accelerator. The method of channeling charged particles occupies an intermediate position in between atomic microscopy and diffraction spectroscopy. Because this method exhibits the precision of diffraction methods, it yields direct information in real space (naturally, for periodic structures) and, unlike atomic spectroscopy, it allows the visualization of large lattice volumes. Moreover, the high energy resolution of electrostatic accelerators provides the possibility of independent investigation of the sublattices of various (including light) elements and their depth profiles by measuring the energy of the detected scattered particles.

Experiments were performed involving inverse scattering of 3.6 MeV helium ions from a monocrystalline Y123 film 1400 Å thick on a support of strontium titanate in the channeling position along the <001> direction. Since the wave function of helium ions, in the case of channeling, is concentrated inside the crystallographic channel, free from nuclei, the intensity of nuclear scattering drops drastically. Here the observed scattering is mainly related to the presence of defects and displacements of nuclei from regular crystallographic positions. It turned out that the distribution of defects is inhomogeneous through the thickness of the film. The quantity of defects is maximal at the surface of the film and on its inverse side adjacent to the support. Extension of defective layers is quite significant and amounts to 400-600 Å. The resonance nature of the scattering of helium ions on oxygen ($E_{res.}$ = 3.045 MeV) permitted clear identification of scattering on the oxygen sublattice, in spite of the high background of scattering from the support. For the first time, the angular width of the oxygen sublattice channeling entrance crater was measured. It turned out that this width is significantly smaller than the crater width of the barium, copper, and yttrium sublattices, which can be explained by the significant dynamic (or static) instability of oxygen in the lattice. Similar investigations will be carried out in the vicinity of the critical temperature of superconductive transition.

The mechanism of radiative formation of defects in YBaCuO monocrystalline films irradiated with helium-4 ions was studied. The influence was determined of the dose accumulated in the course of measurement on the properties of the object being studied. Two aspects were considered: variation of the depth distribution of elements in the film (profiles of elements) under the action of the analyzing ion beam, and destruction during measurement of the crystal lattice being irradiated (Fig. 17). In the case of the YBaCuO film, the contribution of the ionization mechanism amounts to 30-60% of the contribution of collisional defect formation. Simulation of the interaction processes of ions with the atoms of the target resulted in the determination that an average energy of 5 eV is required for an atom of the YBaCuO lattice to be irreversibly substituted.

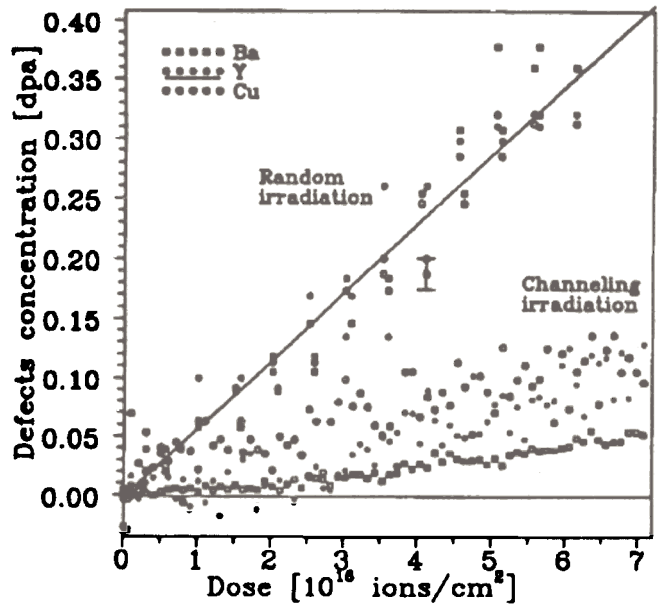

Fig. 17. Dependence of concentration of defects in $YBa_2Cu_3O_7$ film 90 nm thick on the irradiation dose by ^4He ions of 1 MeV energy for chaotic and tunnelled irradiation.

2.2.2. DEVELOPMENT OF THE EXPERIMENTAL BASE

The main event of 1992 turned out to be the beginning of operations of the high resolution Fourier diffractometer (HRFD). It took four years to construct the HRFD in accordance with a joint project of JINR, PINP (Gatchina) and the Centre of Technical Research (Finland). The first run of measurements with the HRFD was carried out in June 1992, just before the summer intermission of the IBR-2 reactor. The idea of realizing the Fourier technique at a pulsed neutron source like the IBR-2 was confirmed to be correct, namely, record parameters of the diffractometer for resolution and luminosity can be obtained with its aid. Routine operation of the Fourier diffractometer started in 1993. Experiments with standard samples (Ge, Al_2O_3) revealed its parameters to be close to the computed ones. Resolution amounted to about 0.0015, which is close to the resolution of the HRFD of RAL (Fig. 18).

The processing of measured diffraction spectra has been organized by using the Rithvield method (Fig. 19) and the first physical experiments were carried out in which HTSC compounds (Y124, Hg-1212) and superproton conductors etc. were studied. A program of applied research has

been initiated with the HRFD. Joint experiments were performed with physicists from the FRG on internal strains in massive objects. A technical base is being created for simultaneous measurement of deformations in two directions perpendicular to each other (the NIDA project).

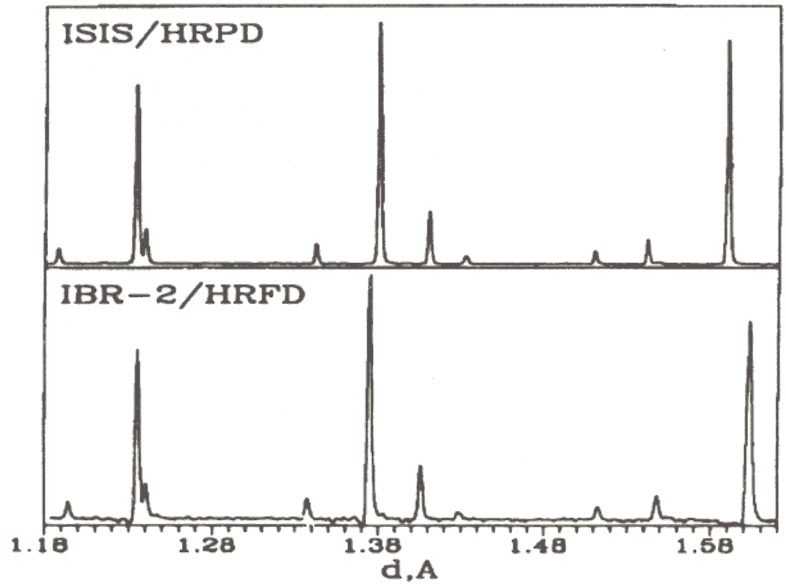

Fig.18. A small section of the Al_2O_3 diffraction patterns measured on the HRPD diffractometer at ISIS (top) and on the HRFD one at IBR-2 (bottom). The horizontal scale is slightly different for the patterns.

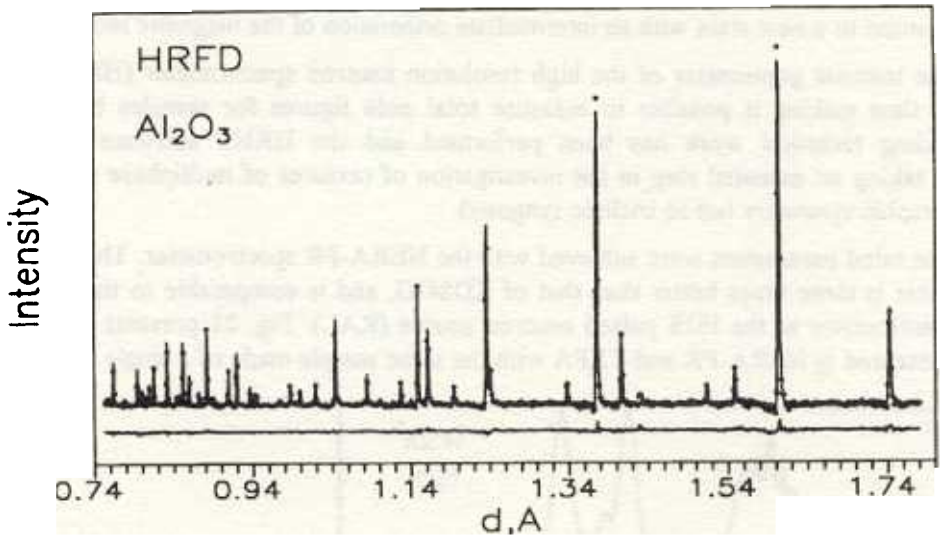

Fig.19. A section of Rietveld refinement pattern for Al_2O_3 measured on the HRFD. As experimental points only every fourth is shown.

A very interesting new study "Investigations at very high pressures" has been initiated at the IBR-2 reactor. The first results have been obtained with the DN-12 diffractometer put into operation in 1993. The idea of DN-12 is based on the peculiarities of observing diffraction by the time-of-flight method at a pulsed neutron source, namely, in the case of an experiment with fixed geometry, there

exists a possibility of detecting diffraction spectra from a polycrystalline sample at a very wide solid angle without significant loss of resolution. To this end it is necessary to use a multidetector detection system with counters located along Debye-Sherer rings.

The first realization of the idea occurred at the beginning of the 1960's, when a diffractometer was constructed at the IBR-1 reactor with a wide-aperture 90° detector (V.V.Nietz, et. al.). The detector of the DN-12 diffractometer represents a circular (360°) set of ^{3}He counters, situated in the vertical plane, and the scattering angle can vary from 45° to 135°. In such geometry effective use of high pressure chambers based on sapphire or diamond anvils is possible, with the primary beam passing through the anvil. Measurements showed the luminosity of DN-12 to exceed by about two times that of the DISK diffractometer at the RNC KI (Moscow) exhibiting a close resolution. In its turn, the luminosity of DISK is several times higher than that of the diffractometers of LLB (Saclay), with which studies are carried out at high pressures, and it approximately corresponds to the POLARIS diffractometer at RAL (England). In principle, this level already permits conducting experiments at pressures of about 100 kbar and to accumulate statistics in reasonable time. The time required for data accumulation from a DyD_3 sample 0.03 mm^3 in volume at a pressure of 80 kbar amounts to about 24 hours (Fig. 20). Experiments with hematite α-Fe_2O_3 at a pressure of 45 kbar confirmed the phase transition to a new state with an intermediate orientation of the magnetic moments.

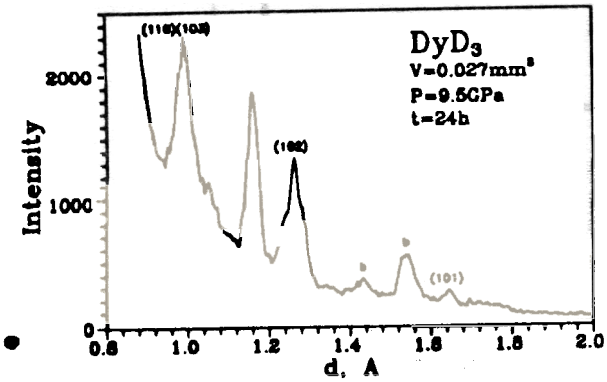

Fig. 20. Diffraction spectrum from DyD_3 measured at a pressure of 9.5 GPa during 24 hours. The sample volume was 0.027 mm^3.

The textural goniometer of the high resolution neutron spectrometer (HRNS) has been re-equipped, thus making it possible to measure total pole figures for samples being studied. The corresponding technical work has been performed and the HRNS software improved, which permitted taking an essential step in the investigation of textures of multiphase materials with low crystallographic symmetry (up to triclinic syngony).

The rated parameters were achieved with the NERA-PR spectrometer. The resolution of this spectrometer is three times better than that of KDSOG, and is comparable to the resolution of the TXFA spectrometer at the ISIS pulsed neutron source (RAL). Fig. 21 presents inelastic scattering spectra measured at NERA-PR and TXFA with the same sample made of a single molecular crystal.

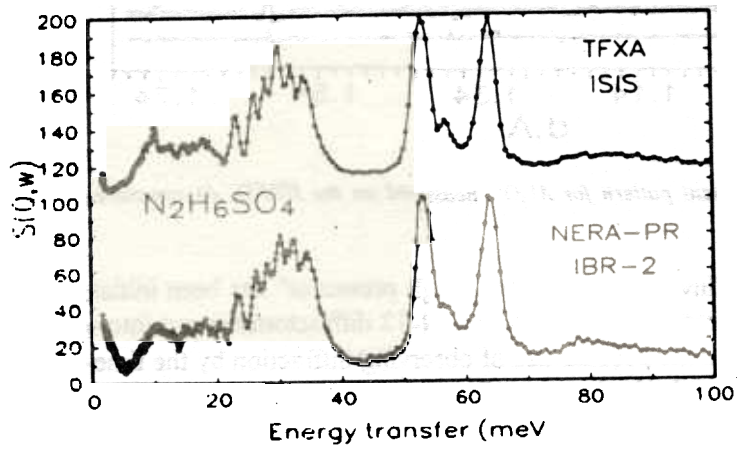

Fig. 21. The high resolution IINS spectra of hydratine sulfate measured on the TXFA (ISIS) and NERA-PR (IBR-2) spectrometers.

Construction of the "Reflex" reflectometric complex at channel 9 of IBR-2 is close to completion. The main mechanical parts of the reflectometer and the storage and measurement electronics have been assembled. The helium cryostat and the magnetic system are close to being completed. Test measurements have estimated fluxes at the sample to be approximately twice the fluxes at the SPN-1 spectrometer operating in the reflectometric mode. Putting the reflectometric complex Reflex-1 (for polarized neutrons) plus Reflex-2 (non-polarized neutrons) into operation will allow essential enhancement of the experimental program for studies of surfaces and thin magnetic and non-magnetic films.

2.2.3. THEORETICAL STUDIES

New theoretical results have been obtained on phase transitions. The freezing temperature $T^*_c > T_c$ for the scalar lattice φ-model of structural phase transitions has been found within the theory of coupled modes. The frequency and temperature dependences of the linear and square susceptibilities have been obtained by self-consistent solution of the equations of coupled modes used for studying the critical behavior of this transition. Two cases have been analyzed: 1) a perfect crystal lattice with a characteristic B-transition at T^*_c, and 2) a system with randomly distributed defects and an A- transition at T^*_c. The experimental aspects of the presented theory are under discussion.

Analysis of the multicomponent order parameter in the $CsHSO_4$ superionic conductor has been carried out. The symmetry of the observed superionic and non-conducting phases was determined and a symmetry of high-pressure phases was predicted.

A number of studies have been conducted in HTSC physics. The spectral density of a hole moving along the AP ground state has been computed within the framework of the Emery model. It has been shown that eigenenergy is nondiagonal in the vicinity of the quasiparticle pole. The mixing of a singlet and triplet depends on the wavevector. Estimation of the optical conductivity has been performed. The results are in good agreement with experimental data and numerical calculations.

The possibility of a self-localized state to form has been examined within the Holstein model. It has been shown that unlike the continual limit, the solution of the Schrodinger equation on a 2D lattice in the adiabatic approximation leads to the formation of a barrier separating self-localized and de-localized states.

The nature of many unusual properties of high-temperature superconductors is due to the existence of a disordered set of weak Josephson links inside them. Within the framework of the model of superconducting granules with randomly distributed phases, it has been shown by renormalizable group methods in replica space that the recurrent Kosterlitz-Tauless transition occurs only for order parameters in the $\pi/8 < A < 1.2\pi/8$ range.

Analysis has been performed of the upper critical field of superconducting super-lattices based on vanadium and copper. It was shown that, owing to a decrease of the magnetic length in strong magnetic fields, a normal metal does not affect the distribution of the superconducting nucleus in the super-lattice. Numerical computation of the Ginzburg-Landau equation is in good agreement with experimental data. Analysis has been performed of the temperature dependence of the line width for transitions between f-levels of Tm ions split by a crystalline field in YBCO. It has been shown

that the main contribution to the broadening is due to antiferromagnetic fluctuations in the vicinity of the G-point of the Brillouin zone, while the temperature dependence is determined by the static susceptibility. Numerical analysis has been performed of the strongly interacting phonon-electron system. It was shown that the exact solution coincides with the adiabatic Holstein polaron. Exact diagonalization was applied to calculations of an optical polaron of small radius, which can be done only in the limit of strong coupling.

The problem of reconstructing the distribution of internal magnetic fields from the depolarization function observed for a polarized neutron beam on its passage through a magnetic medium is very important. A new approach, based on the model of strong interaction, has been developed for computation of the depolarization function. The results of the Halpern-Holstein theory are reproduced for the limit of small wavelengths. Investigation of the specular reflection of neutrons from various types of multilayers is one of the important practical issues of constructing mirrors for neutron guides. Numerical analysis has been performed of the neutron reflection coefficient from multilayer structures, forming a sequence of so-called Fibonacci layers. It has been shown that disorder of the quasicrystalline type in how the materials of the mirrors are arranged may result in a shift of the neutron backscattering region toward either longer or shorter wavelengths.